Applied Catalysis B: Environmental 148–149 (2014) 1–10

Contents lists available at ScienceDirect

Applied Catalysis B: Environmental

journal homepage: www.elsevier.com/locate/apcatb

Effect of metal oxides concentration over supported cordierite monoliths on the partial oxidation of ethanol

J.A. Gómez-Cuaspud, M. Schmal*

NUCAT/COPPE/UFRJ, Centro de Tecnologia, Bloco G, sala 228, CEP 21945-909 Rio de Janeiro, RJ, Brazil

ARTICLE INFO

Article history:
Received 29 July 2013
Received in revised form 15 October 2013
Accepted 17 October 2013
Available online 25 October 2013

Keywords:
Metaloxides
Ethanol oxidation
Monoliths

ABSTRACT

The effect of metal oxide concentration supported over monoliths was studied on the partial oxidation of ethanol. Nano-structured Co_3O_4, NiO and CuO oxide catalysts were prepared by means of polymerization–combustion technique using citric acid as chelating agent and washcoated over cordierite monoliths, which after combustion process were calcined and tested under isothermal conditions. X-ray diffraction (XRD) and high resolution transmission electronic microscopy (TEM) showed nanostructure and stable crystallite materials. These metal oxides were tested in the partial oxidation reaction, showing that metal oxide concentration influences the product distribution and selectivity. The maximum concentration for all samples was 12% of corresponding metal oxide (MeO), resulting in high conversions and H_2 selectivity. Diffuse reflectance infrared Fourier transform spectroscopy of adsorbed ethanol (DRIFTS-EtOH) and TPD desorption of ethanol showed the formation of intermediate ethoxy-species and preferential dehydrogenation reaction.

1. Introduction

Hydrogen production from bio-ethanol by steam reforming (SRE) and partial oxidation of ethanol (POE) are gaining increasing attention and may become important industrial process [1,2]. Ethanol has several advantages compared to other raw materials, but the most important is its renewable nature and subsequent overall reduction in CO_2 emission. An additional benefit of POE is related with the fact that process can be ran under autothermal conditions, thereby is possible to eliminate the need for external heat. Moreover, is much faster than catalytic steam reforming, allowing a quick start-up and short response times [3].

Generation of hydrogen from ethanol via catalytic partial oxidation has been studied under several temperature ranges from 450 to 900 °C using catalytic systems based on noble metals and rarely based on nickel or cobalt. Although supported noble metal catalysts have shown high activity and stability [4–6], supported nickel and cobalt catalysts are available at much lower cost. Currently, the most important task in POE research is identification of economic and stable catalysts.

Ethanol partial oxidation follows a very complex pathway, including several reaction intermediates formed and decomposed on both, supports and active metals comprising the catalytic systems. The nature of the support and the metal directly influences product distribution and catalyst stability during ethanol conversion reactions [7,8]. Several active phases have been proposed to serve as catalyst for this reaction [9,10].

Catalyst efficiency is one of the most important aspects in partial oxidation of ethanol (POE), since it is directly related with concentration of active catalytic phase. The use of transition metal oxides have been investigated by several authors and among the most important catalyst Co, Ni and Cu oxides representing the most active, selective and low cost materials for eventual applications. Recently the literature [11] reported the behavior of different catalysts for the partial oxidation of ethanol (POE), suggesting the promotion of dehydrogenation and dehydration reactions.

The use of different metal oxides concentration supported on alumina, indicates that high concentrations did not affect the activity and selectivity [12–16]. There are several publications reported in the literature related to the hydrogen production from ethanol, using nickel, cobalt, copper, chrome, noble metals and other catalytic metallic oxides as powders, pellets and ceramic foams, fed with water/ethanol mixtures with the main objective to identify some important catalytic aspects for the hydrogen production and high added-value products [13–20]. The partial oxidation of ethanol was studied under isothermal conditions based on previous thermodynamic predictions [21–23].

Based on these facts, we focus our investigation on systems derived from Co, Ni and Cu oxides, varying the metal oxide

* Corresponding author. Tel.: +55 21 2562 8352; fax: +55 21 2562 8300.
E-mail address: schmal@peq.coppe.ufrj.br (M. Schmal).

0926-3373/$ – see front matter © 2013 Elsevier B.V. All rights reserved.
http://dx.doi.org/10.1016/j.apcatb.2013.10.036

concentration supported over γ-Al_2O_3/cordierite monoliths for the partial oxidation of ethanol, and the relationship between the physicochemical and catalytic properties. Additionally, study the effect of synthesis, using citric acid to form metal–organic complexes that seems to be an effective way to obtain active and selective materials for this reaction with satisfactory stability, carbon resistance and anti-sintering properties in comparison with traditional catalyst prepared by the solid state technique. Finally, we study the influence of the metal oxide concentration on the activity and selectivity of unreduced metal oxides and the stability for the partial oxidation of ethanol reaction under isothermal conditions at low and high temperatures.

2. Experimental

2.1. Preparation of catalysts

The honeycomb cordierite monoliths have a cell density of 400 cells in-2 (D = 12 mm, L = 8 mm). The catalyst was prepared by washcoating of different metal oxides over γ-alumina. The γ-alumina support was prepared with a transition alumina solution using methods described elsewhere [24] and dipcoated over monoliths as described previously [25–27].

The active phases of Co_3O_4, NiO and CuO were prepared by polymerization–combustion technique, starting from the corresponding nitrates $Co(NO_3)_2{\cdot}6H_2O$ (99.9%), $Ni(NO_3)_2{\cdot}6H_2O$ (99.9%) and $Cu(NO_3)_2{\cdot}9H_2O$ (99.99%), using citric acid monohydrated (99.99%). Stoichiometric quantities of each solid salt (0.01 mol) were added to 20 mL of absolute ethanol in different glass vessels, equipped with magnetic stirring (150 rpm), reflux system and temperature control, as described elsewhere [20]. Once reached complete dissolution of each precursor, citric acid was added at 0.5:1 molar ratio with respect to the total concentration of metal cation in dissolution. Several solutions of 0.5 molar concentrations were kept under reflux at 120 °C for 12 h, until formation of a viscous liquid, which was then impregnated on cordierite honeycombs for each case. After washcoating the monoliths were heated at 150 °C under air flux in an oven until complete solvent evaporation and calcined at 500 °C under oxygen flow for 4 h to eliminate carbonaceous residues. The excess was removed using an ultrasonic cleaner after completing several deposition cycles with 3, 12 and 25 (%, w/w), respectively, as reported previously [24]. These samples were kept in a chamber under controlled humidity (20%) before catalytic testing. The stoichiometric composition was calculated based on the total oxidizing and reducing valences (N/C), assuming total combustion of citrate species.

$$(NO_3)^- + C_6H_{18}O_7 \rightarrow 6CO_2 + N_2 + 9H_2O + \text{oxides} \quad (1)$$

2.2. Characterization of catalysts

The chemical composition was obtained by X-ray fluorescence (XRF) technique, using an apparatus Rigaku Model RIX 3100. Samples were pressed as pellets and analyzed quantitatively. The specific area BET was evaluated by nitrogen adsorption isotherms at −196 °C, using an ASAP-2020 apparatus (Micromeritics). All samples were degassed at 350 °C overnight to remove residual humidity.

The crystalline structure was determined by X-ray diffraction, in a Miniflex Rigaku diffractometer, using Cu K_α radiation (λ = 1.54186 Å) between 10° and 90°, with steps of 0.05° and a speed analysis 0.15° min^{-1}. Refinement, indexing and the simulation of the structures were done with MAUD software that allowed establishing the chemical composition and crystallographic structure of the oxides. The crystallite sizes were calculated using the highest diffraction signals, using the Debye–Scherrer equation, taking the value of half peak width set by a Lorentzian function and using a constant of 0.89 as reference.

Temperature programmed reduction (TPR-H_2) was performed in a Micromeritics Pulse Chemisorb model 2705 equipment. The sample was heated at 200 °C for 2 h, flowing pure helium and then reduced with a mixture of 5% H_2/He (30 mL min^{-1}), rising up to the maximum temperature reduction at 10 °C min^{-1}. The H_2 consumption was measured using a thermal conductivity detector.

Scanning electron microscopy analysis (SEM) was performed using a LEO 440 microscope (Leica, Zeiss), equipped with an electron gun and a spectrometer measuring the energy dispersive X-ray. Images were obtained with a focus distance of 10–25 mm, an accelerating voltage of 20 kV and a current of 100–200 pA, measurement time of 100 s and count rate of 1.2 kcps. The samples were placed on a graphite holder bonded to a carrier of aluminum and shadowed with platinum to obtain a better contrast in the images.

Transmission electronic microscopy analysis (TEM) was performed on a JEOL 2100 equipment using a LaB_6 thermionic gun operated with an acceleration voltage of 200 kV, equipped with a CCD imaging system. For analysis, these samples were ground to obtain fine powders, which were sieved to 200 U.S. standard mesh and dispersed in a test tube with 5.0 mL of water and each tube was placed in a ultrasonic equipment for a period of 30 min, after which a drop of the top of each tube was taken and dried at 45 °C for respective analysis.

Diffuse reflectance infrared Fourier transform spectroscopy of ethanol adsorption (DRIFTS-EtOH) was carried out on a Nicolet spectrometer (Nexus 470 model), with a MCT detector and equipped with a diffuse reflectance chamber (Spectra Tech) for high temperature treatment. The *in situ* treatment was carried out using a feed composition of $C_2H_5OH + O_2$ (1:0.5 mL min^{-1}), which was analyzed at different temperatures (100, 200, 300 and 400 °C), using different residence times and collecting 150 spectrums per point.

Volumetric CO and H_2 chemisorption was performed in the ASAP-2020 Micromeritics equipment, using the volumetric technique. All samples were pretreated before adsorption and reduced at 500 °C for 1 h, under H_2 flow (50 mL min^{-1}). After reduction, sampler was evacuated for 1 h at 400 °C and cooled down at adsorption temperature under vacuum. Irreversible uptakes were determined from dual isotherms measurements for hydrogen at 150 °C and carbon monoxide at room temperature, according to the methodology described elsewhere [28]. To evaluate the metal surface, we used the following expression:

$$S_m = \frac{N_s}{[L]} \quad (2)$$

where $[L]$ is the maximum density of sites or the number of surface metal atoms per m^2 and N_s is the number of surface sites, or the number of chemically adsorbed molecules. Considering the level of metal:

$$S_m = \frac{N_s}{y[L]} \quad (3)$$

For calculation of dispersion percentage, we used the expression:

$$D(\%) = \frac{N_s}{N_t} \cdot 100 \quad (4)$$

where N_t is the total number of atoms given by following expression:

$$N_t = \frac{y m_{cat}}{M} \cdot N_A \quad (5)$$

where N_A is Avogadro's number, y the fraction of supported metal, m_{cat} is the mass of catalyst and M is the atomic weight of metal.

2.3. Catalytic test

The MeO/γ-Al_2O_3/cordierite monoliths (10 mm × 8 mm) were tested for the ethanol partial oxidation (absolute ethanol P. A. Merck). The reaction was performed in an experimental unit consisting of a set of mass flowmeters (MKS) and a reactor coupled to a resistive furnace. The liquid was pumped to a vaporizer, heated at 160 °C and then mixed with the gas stream. The reactor consists of a U shape quartz microreactor with 12 mm ID and 250 mm long. The monoliths were supported over quartz wool.

The monoliths were dried at 350 °C for 30 min prior catalytic tests under helium flow (30 mL min^{-1}). In our previous work the catalytic performance was evaluated after reducing the catalyst with pure hydrogen for 2 h at 500 °C and without pretreatment. As observed there is no difference among catalyst performance indicating that the catalyst undergoes to activation at the reaction conditions [20]. Therefore, the samples were used in the oxide form. After cleaning and cooling, the gas valve was switched to the gas mixture and adjusted until stabilization. The feed composition was 8 O_2, 42 He and 0.1 EtOH (mL min^{-1}), GSHV = 18,000 h^{-1} and a contact time of 0.20 s. The reaction was studied under isothermal condition at 420 and 650 °C and exit gases were analyzed by gas chromatography (Trace GC Ultra, Thermo Electron Corp) equipped with a Mol Sieve (3 m 60/80) and capillary columns CP Wax 52 CB (50 m × 0.32 mm) using a TCD detector operated with He and a TCD detector operated with N_2. Finally, the FID flame detector allowed to evaluate the conversion of EtOH, O_2 (X_{EtOH}, X_{O_2}), the selectivity (S_{CO}, S_{H_2}) and the most important products derived from the reaction.

The main products from the partial oxidation reaction were hydrogen, methane, carbon dioxide, carbon monoxide, ethylene, ethane, acetaldehyde and diethyl ether. The conversion of ethanol was calculated from carbon products in molar balance (on dry basis), presented in Eq. (6) where $\boldsymbol{\gamma_{Ci}}$ is the ratio of carbon content of product $\boldsymbol{i}$ to carbon content of ethanol molecule, and $\boldsymbol{y_{Ci}}$ is the molar fraction of carbon content products in the effluent flow [29]. The molar selectivity was defined as the ratio of moles of one product and the total moles of products, based on experimental values.

$$X_{\text{Ethanol}}(\%) = \frac{\sum \gamma_{Ci} y_{Ci}}{y_{\text{Ethanol}} + \sum \gamma_{Ci} y_{Ci}} \times 100 \quad (6)$$

3. Results and discussion

3.1. Catalyst preparation and characterizations

Chemical composition was calculated by X-ray fluorescence after impregnation, as presented in Table 1. These results are close to the nominal values 3, 12 and 25% of Co, Ni and Cu oxides, respectively.

The specific surface areas (S_{BET}, $m^2\ g^{-1}$) of pure oxides are presented in Table 2 and compared with the specific area of γ-Al_2O_3. Results show that the initial surface areas are high, but decreased with increasing amount of oxides, when compared to alumina support. The surface area of the Co_3O_4 sample was less affected, which can be attributed to the lower auto-combustion temperature in the synthesis process; all samples were pre-treated at 300 °C, but the auto-ignition of the cobalt oxide sample started up before at lower temperature, followed by nickel and copper oxides, respectively, releasing nitrogen oxide gas in the course of thermal dissociation of the nitrate precursors. In fact, this provoked a decreasing surface area of NiO and CuO catalysts, probably due to the thermal treatment for long heating time (4 h) at 500 °C, which might induce growth of the metal oxide particles.

Table 1
Elemental composition of metal oxides derived from X-ray fluorescence analysis.

Catalyst oxide	Cobalt			Nickel			Copper		
	3.0	11.9	25.0	3.0	11.9	24.8	2.9	11.6	24.8
Al_2O_3	44.2	40.4	34.2	44.2	40.2	34.9	43.5	40.3	34.7
SiO_2	41.2	37.3	31.9	41.3	37.3	31.8	40.6	37.7	31.7
MgO	11.5	10.4	8.9	11.5	10.5	8.5	12.6	10.4	8.5
Total (100%)	99.9	100	100	100	99.9	100	99.6	100	99.7

Table 2
Surface area of obtained metal oxides supported over γ-Al_2O_3 at different percentages.

Catalyst (%, w/w)	Surface area (m^2/g)		
	Cobalt	Nickel	Copper
3	196	187	181
12	174	155	165
25	132	101	91
γ-Al_2O_3	225		

XRD patterns of Co_3O_4, NiO and CuO supported oxides after polymerization–combustion are shown in Fig. 1. Results indicate crystalline structure of the corresponding oxides with the most important reflection signals. The results confirm the presence of these supported oxides, as displayed in Fig. 1. Using the Xípert High Score software it was possible to confirm the presence of the main diffraction signals related with Co_3O_4 (JCPDS: 42-1467), NiO (JCPDS: 89-5881) and CuO (JCPDS: 45-0937) oxides, in accordance with literature [30].

Crystallite sizes were estimated using the highest diffraction lines and Debye–Scherrer equation, taking the value of half peak width ($\boldsymbol{\beta}$), adjusted to a Lorentzian function and using a constant of 0.89 as reference, indicating the presence of nanometric crystallites. Using ICCD databases we calculated space groups, crystal systems and cell parameters for each oxide, as shown in Table 3.

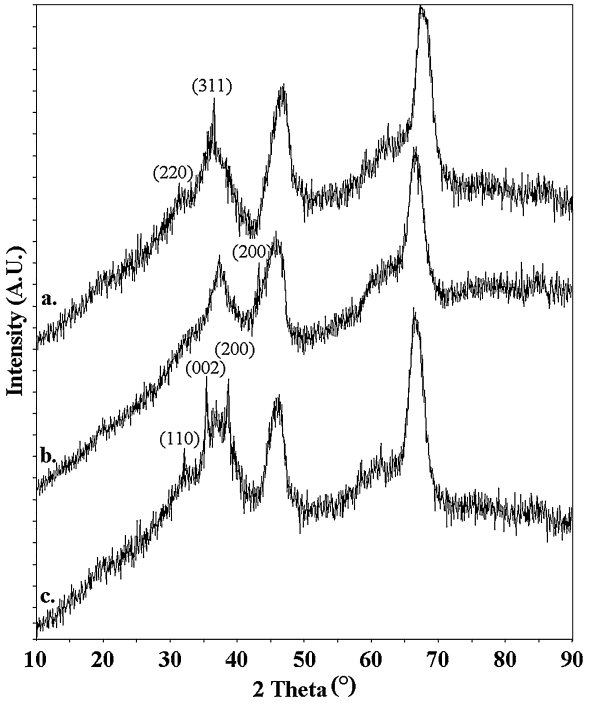

Fig. 1. X-ray diffraction patterns for (a) Co_3O_4, (b) NiO and (c) CuO supported oxides.

Table 3
Crystalline properties of obtained supported oxides.

Catalyst	Average crystallite size (nm)	Space group	Crystal system	Cell parameters
Co_3O_4	39.8	*Fd−3m* (227)	Cubic	$a = 8.056\,Å$
NiO	34.3	*Fm−3m* (225)	Cubic	$a = 4.177\,Å$
CuO	42.9	*C2/c* (15)	Monoclinic	$a = 4.690$ Å, $b = 3.420$ Å, $c = 5.131$ Å, $\beta = 99.54°$

The crystallite sizes are quite similar; $d_c = 39.8$ nm; 34.3 nm and 42.9 nm for Co_3O_4, NiO and CuO, respectively. Thus, the catalysts prepared by means of polymerization–combustion route promote the stabilization of nanometric phases in contrast with the same catalysts prepared by the traditional thermal treatment of nitrate salts [30].

The TPR-H_2 profiles of Co_3O_4, NiO and CuO oxides are shown in Fig. 2. The maximum reduction signal of Co_3O_4 occurred at 390 °C with a shoulder around 300 °C. According to Khodakov [31] the reduction of unsupported Co_3O_4 could be ascribed to successive reduction, one at low temperature between 100 °C and 350 °C, which is commonly assigned to partial reduction of Co_3O_4 or reduction–decomposition in hydrogen of residual cobalt precursors and then, the reduction at higher temperature, attributed to the reduction of Co^{2+} species to metallic Co^0. Enache [32] has observed different reduction peaks between 400 °C and 600 °C on supported catalysts which do not occur in this sample prepared by means polymerization–combustion technique. The reduction occurs, according following reactions:

$$Co_3O_4 + H_2 \rightarrow 3CoO + H_2O \quad (7)$$

$$3CoO + 3H_2 \rightarrow 3Co^0 + 3H_2O \quad (8)$$

The TPR-H_2 profile of NiO oxide displays a maximum reduction peak at 359 °C with a shoulder around 300 °C. The reducibility of the nickel based-catalysts has been extensively studied by TPR. Based on the reduction temperature, different nickel species can be found. Up to 330 °C it is attributed the reduction of bulk nickel oxide to metallic Ni^0. The shift of the main peak to lower temperatures can be associated with the maximum temperature reached during the combustion process. Comparing the reduction of NiO prepared by the conventional method it turns out that the maximum peak is shifted to lower temperature from 502 °C to 359 °C. The reduction at lower temperature is attributed to the reduction of non-stoichiometric Ni_2O_3 species to NiO, which resulted from the preparation method. The TPR-H_2 profile of CuO sample exhibits one maximum peak at 230 °C, which is related with reduction of bulk copper oxide to Cu^0 [30].

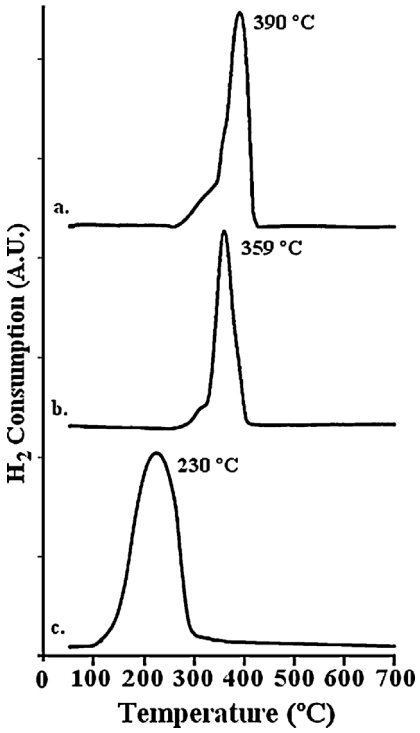

Fig. 2. TPR-H_2 profiles for (a) Co_3O_4, (b) NiO and (c) CuO supported oxides (10% H_2-He ramping rate 10 °C min^{-1}).

SEM observations are displayed in Fig. 3, showing at different magnifications, some morphological and surface characteristics. At microscopic level, the solids are composed by irregular aggregates, distributed with particle sizes between 0.5 μm and 200 μm. In principle, these pictures are related with the texture and the relief created by elimination of solvent during the combustion of organic compounds after thermal treatments. In the same sense, it is remarkable that these materials present some degree of densification, favoring a compacted morphology.

Results derived from transmission electronic microscopy (TEM) allowed a statistical counting in all micrographs obtained by reference in a population of 200 particles per material and based on the Eq. (9), where $\boldsymbol{n_i}$ represent the number of particles and $\boldsymbol{d_i}$ represent the particle diameters.

$$d = \frac{\sum_i n_i d_i^3}{\sum_i n_i d_i^2} \quad (9)$$

The data were recollected and normalized obtaining regular distributions of crystallite sizes with regular morphology and characteristic interplanar distances for each system in the principal reflection planes, as shown in Fig. 4.

These results confirm previous analyses derived from X-ray diffraction, where nanometric aggregates were identified, providing several catalytic advantages in terms of activity. Fig. 5 displays the histograms of particle size distribution for the supported systems, showing in each case an unimodal distribution with a marked Gaussian behavior which reveals the presence of nanometric particles in the range of 38.2 to 41.2 nm. These results are favored by the low temperature of calcination after self-combustion process.

From high resolution transmission electronic microscopy data and X-ray diffraction analysis, it was possible to calculate the units cell of each oxide system, by means the use of ELMIX software. This software allowed establishing from experimental images a simulation of crystalline parameters, as shown in Fig. 6 and Table 4.

Results are in agreement with those derived from X-ray diffraction and transmission electronic microscopy, and therefore we conclude that this software used for calculation of crystalline parameters is an effective method for complementing experimental results.

Chemisorption in Table 5 represents the metallic dispersion results for all catalysts. There are significant differences in terms of CO adsorption, metallic areas and metal dispersions. The Co_3O_4 sample exhibited the highest metallic surface area and metal dispersion in comparison to NiO and is 4 times higher than the CuO.

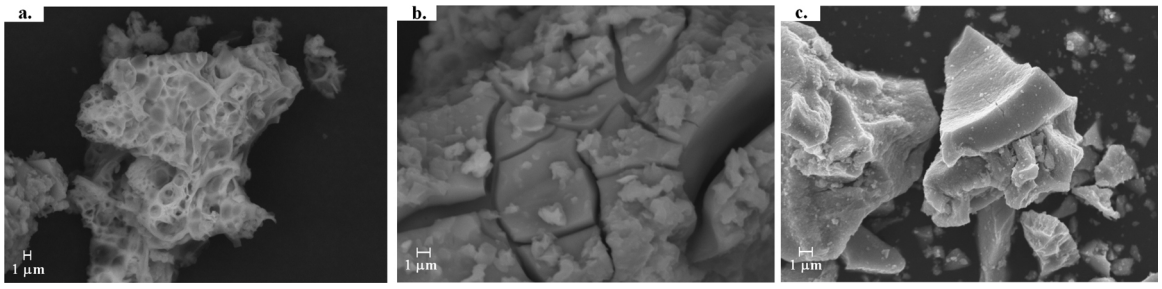

Fig. 3. Scanning electron microscopy images for (a) Co_3O_4, (b) NiO and (c) CuO supported oxides.

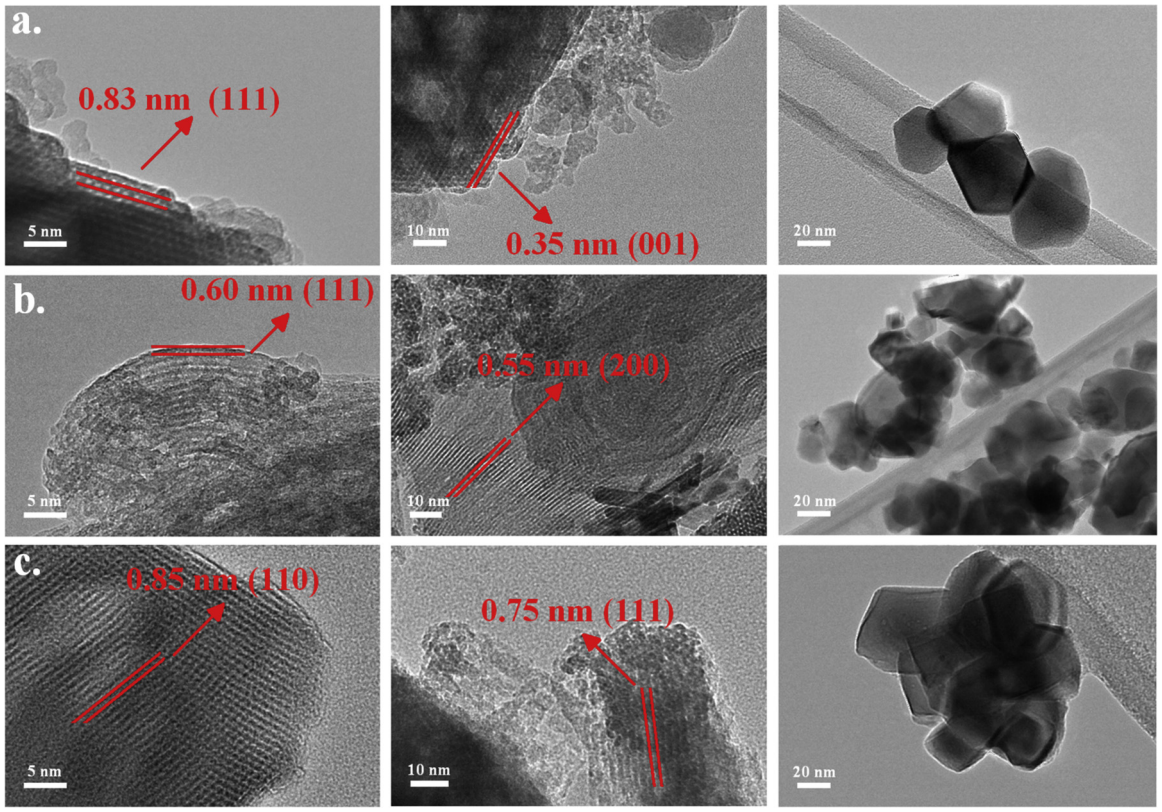

Fig. 4. Transmission electron microscopy images for (a) Co_3O_4, (b) NiO and (c) CuO supported oxides.

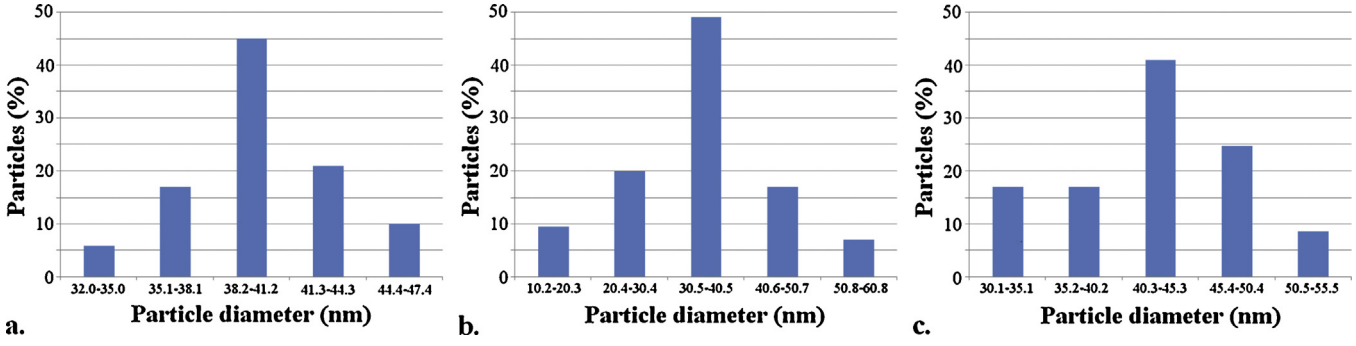

Fig. 5. Particle size distribution data determined from transmission electron microscopy on supported oxides of (a) Co_3O_4, (b) NiO and (c) CuO.

Table 4
Some crystalline properties derived from simulation images using ELMIX software.

Catalyst	Average crystallite size (nm)	Space group	Crystal system	Cell parameters
Co_3O_4	36.0	*Fd−3m*	Cubic	$a = 8.09$ Å
NiO	31.0	*Fm−3m*	Cubic	$a = 4.21$ Å
CuO	45.0	*C2/c*	Monoclinic	$a = 4.50$ Å, $b = 3.40$ Å, $c = 5.10$ Å, $\beta = 99.50°$

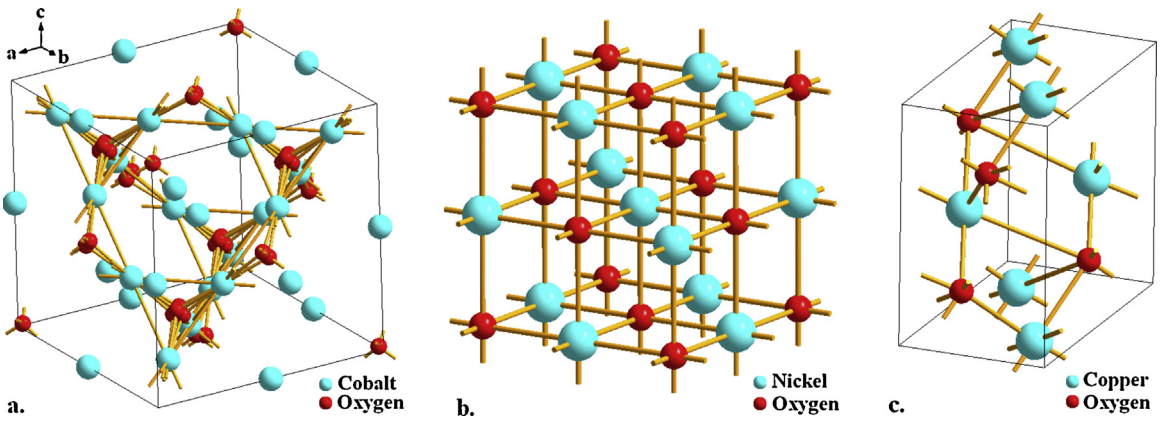

Fig. 6. Unitary cells of (a) Co_3O_4, (b) NiO and (c) CuO oxides calculated using ELMIX software.

Table 5
CO chemisorption values for obtained materials.

Catalysts	Metallic content (%)	μmolCO/g_{cat}	S_m (m^2/g_{metal})	k (g_{metal}/m^2s)
Co_3O_4	12.1	64.4	49.2	0.118
NiO	12.5	53.8	36.9	0.110
CuO	12.3	15.2	11.1	0.420

3.2. Activity and selectivity

Catalytic tests were carried out for different concentrations of Co_3O_4, NiO and CuO supported on γ-Al_2O_3 washcoated on cordierite monolith honeycombs (10 mm × 8 mm). Results are shown separately in Table 6 for Co_3O_4/γ-Al_2O_3/cordierite, NiO/γ-Al_2O_3/cordierite and CuO/γ-Al_2O_3/cordierite. Reaction temperature was kept at 420 °C and space velocity GSHV = 1.8×10^4 h^{-1}.

3.2.1. Co_3O_4/γ-Al_2O_3/cordierite catalysts

The ethanol conversion increased with increasing metal content of Co_3O_4 reaching a maximum conversion of 68% for 12%Co_3O_4, decreasing than for higher concentrations (25%Co_3O_4). Rodrigues et al. [24] obtained 52.5% conversion for 6% Co_3O_4 at 420 °C under similar reaction conditions.

The selectivity for different Co_3O_4 concentrations is presented in Table 6. The H_2 selectivity for 12% Co_3O_4 catalyst increased 3 times and the conversion is doubled compared to the sample with lower content 3% Co_3O_4 catalyst. Besides, the selectivity of acetaldehyde diminished with increasing concentration from 35.7% for 3% Co_3O_4 to 23.8% for 25% Co_3O_4, reaching a minimum value of 20.9% for 12% Co_3O_4, besides the formation of ethylene and diethyl ether, suggest preferential dehydrogenation and dehydration reactions. The CO_2/CO ratio decreased with increasing metal content and higher conversions. In fact, the formation of CO indicates the occurrence of the reverse water gas shift reaction (Eq. (20)).

3.2.2. NiO/γ-Al_2O_3/cordierite catalysts

The ethanol conversion for the NiO/γ-AlO_3 catalyst under similar conditions is lower than for the cobalt catalyst, but the hydrogen selectivity decreased. The oxygenated products did not change significantly with increase of metal oxide contents. Rodrigues et al. [20] obtained 56%, ethanol conversion and 4.4% H_2 selectivity for similar conditions. However, for lower NiO concentration (6%, 12%

Table 6
Ethanol conversion and product distribution on partial oxidation of ethanol over (a) Co_3O_4, (b) NiO and (c) CuO/γ-Al_2O_3/cordierite catalysts at 420 °C and GSHV = 1.8×10^4 h^{-1}.

Co_3O_4										
% (w/w)	$X_{ethanol}$ (%)	CO_2/CO	Selectivity (% molar)							
			H_2	CH_4	CO	CO_2	CH_2=CH_2	CH_3CHO	C_2H_6O	CH_3COOH
3	33.6	1.20	5.9	11.9	17.4	12.1	9.3	35.7	5.3	2.4
12	68.9	0.78	17.9	24.7	15.1	9.8	6.5	20.9	2.1	3.0
25	65.4	0.37	13.0	19.1	14.6	10.6	9.9	23.8	1.6	7.4
NiO										
% (w/w)	$X_{ethanol}$ (%)	CO_2/CO	Selectivity (% molar)							
			H_2	CH_4	CO	CO_2	CH_2=CH_2	CH_3CHO	C_2H_6O	CH_3COOH
3	35.3	1.00	6.7	12.9	15.6	12.0	10.3	28.1	8.5	5.9
12	55.9	0.90	8.4	17.6	19.2	11.9	8.7	23.3	4.0	6.9
25	54.5	0.90	8.3	17.5	18.9	11.5	9.0	22.9	6.1	5.8
CuO										
% (w/w)	$X_{ethanol}$ (%)	CO_2/CO	Selectivity (% molar)							
			H_2	CH_4	CO	CO_2	CH_2=CH_2	CH_3CHO	C_2H_6O	CH_3COOH
3	35.3	0.89	6.1	11.7	16.1	14.1	6.3	45.2	0.5	0.0
12	60.7	1.15	9.3	19.5	18.2	11.0	9.2	25.3	0.0	7.5
25	68.2	1.11	8.9	20.1	18.4	13.2	8.5	24.9	0.4	5.6

NiO/γ-Al_2O_3), the conversion was equal (55.9%) while the H_2 selectivity doubled.

3.2.3. CuO-γ/Al_2O_3/cordierite catalysts

The conversions are quite similar to the Co_3O_4/γ-Al_2O_3 catalyst, as shown in Table 6. However, the selectivity containing carbon changed, presenting 31% acetaldehyde, and 38% of CO, CO_2 and ethylene, for similar conversion (54%). Indeed, the primary products ethylene and acetaldehyde resulted from the dehydrogenation and dehydration reactions of ethanol (Eqs. (12) and (13)), while CO and CO_2 as byproducts from the partial oxidation of ethanol and the water gas shift (Eqs. (10) and (11)).

$$C_2H_5OH_{(v)} + (1/2)O_{2(g)} \rightarrow 2CO_{(g)} + 3H_{2(g)} \quad (10)$$

$$CO_{(g)} + H_2O_{(v)} \leftrightarrows CO_{2(g)} + H_{2(g)} \quad (11)$$

$$CH_3CH_2OH_{(v)} \rightarrow CH_3CHO_{(l)} + H_{2(g)} \quad (12)$$

$$C_2H_5OH_{(v)} \rightarrow C_2H_{4(g)} + H_2O_{(v)} \quad (13)$$

3.3. Specific activity

The specific activity in terms of metallic surface area can be calculated, considering a first order reaction, assuming an integral reactor, since the conversions are relatively high. Thus, the specific rate constant is according to Eq. (14):

$$k^* = kS_m = -\left(\frac{1}{\tau}\right)\ln(1-x) \quad (14)$$

where the space time is $\tau = 0.2\ s^{-1}$. With the experimental conversions, presented in Table 5, we calculated the specific rate constants for all catalysts with 12% concentration that exhibited the best performance in terms of conversion and selectivity.

The results of k are presented in the last column of Table 5. Noteworthy is that the intrinsic activities for the Co_3O_4 and NiO catalysts are equal, while for the CuO catalyst higher by a factor of 3. In fact, all catalysts presented similar specific activities, depending on the metal oxide exposed at the surface. The metallic surface area of CuO is relatively low, probably due to the formation of carbonate species reducing the effective metal oxide surface area.

3.4. Stability test

Stability test were performed during 5 days, using the three supported catalyst of Co_3O_4, NiO and CuO with 3, 12 and 25% under similar reaction conditions. Results are displayed in Fig. 7. The 25% Co_3O_4/γ-Al_2O_3/cordierite sample deactivated with time on stream after 24 h, decaying progressively between 20% and 40%, while the hydrogen production or selectivity did not change after 120 h. However, the catalysts with 12MeO/γ-Al_2O_3/cordierite catalysts are very stable for all metal oxides, reaching ethanol conversions of 68% for Co_3O_4, 55% for NiO and 58% for CuO. The lower content, 3 MeO/γ-Al_2O_3/cordierite catalyst showed fast deactivation and the final conversions were similar, 37% for NiO, 30% for Co_3O_4 and 28% for CuO. Indeed, these results evidence that optimal concentration for the metal oxides supported over MeO/γ-Al_2O_3/cordierite catalysts is 12%, exhibiting high stability with time on stream, while higher concentrations show fast deactivation due to carbon formation at the surface and unlikely byproducts.

Carbon analyses of spent samples after reaction presented a large amount of carbon deposition, in particular for 25% Co_3O_4. The final carbon content was 79.5% (%w) in comparison with fresh catalyst. According to literature, it is attributed to the dehydrogenation of ethanol, forming acetaldehyde that decomposes in methane and undergoes steam reforming. However, the second way is by means of dehydration of ethanol forming ethane and rupture of C—C bonds that produce coke. In fact, cobalt oxide catalysts are very active and selective for steam reforming of ethanol. However, the disadvantage is the fast deactivation by coke deposition. Deactivation can be attributed to the formation of carbides and carbon at the surface.

4. Discussion

The influence of the metal oxide content on the selectivity and product distribution with conversion is displayed in Fig. 8. Results at 420 °C show that the hydrogen selectivity increases with conversion, reaching a maximum for 12%MeO, decreasing rapidly with higher metal oxide contents. The highest selectivity was obtained for Co_3O_4 (70% conversion), showing that the metal content affects among others, the methane selectivity. Fig. 8c displays the product distribution of ethylene, acetaldehyde and acetic acid, reaching minimum conversion for 12% Co_3O_4, enabling the formation of larger amounts of hydrogen. Rodrigues et al. [24] obtained 50% selectivity for acetaldehyde at 420 °C for 52.5% conversion and for 6% Co_3O_4, evidencing the influence of the metal oxide content on the ethanol dehydrogenation reaction. However, above 12% metal oxide content the selectivity changed significantly, which can be attributed to the dehydrogenation and water gas shift reactions, as shown in Eqs. (eqs. (11) and (12)) respectively. In addition, the selectivity of methane is low, favoring the steam reforming reaction of methane (Eq. (15)), increasing significantly the H_2 selectivity.

$$CH_{4(v)} + H_2O_{(v)} \rightarrow 3H_{2(g)} + CO_{(g)} \quad (15)$$

Ethyl ether was observed at the beginning due to the dehydration reaction, disappearing after 2 h, while ethylene decreased initially with time on stream, but remains constant. Rodrigues et al. [24] did not observe formation of ethylene above 400 °C. In fact, according to the literature, cobalt is active for the dehydrogenation reaction of ethanol to acetaldehyde that in the presence of steam favored the reforming reaction. Llorca et al. [33] showed that cobalt oxide is responsible for the activation of the dehydrogenation reaction of ethanol, promoting the reduction to metallic cobalt under reaction conditions, favoring reforming of both ethanol and acetaldehyde. However, oxygen oxidizes the metallic cobalt particles, favoring the acetaldehyde production.

Indeed, the main products methane, ethylene and acetaldehyde derived from the dehydrogenation and dehydration reactions (Eqs. (12 and 13)) and CO and CO_2 from the partial oxidation of ethanol, the water gas shift (Eqs. (10 and 11)) and the ethanol decomposition reactions in the gas phase (Eq. (16)).

$$CH_3CH_2OH_{(v)} \rightarrow CH_{4(g)} + CO_{(g)} + H_{2(g)} \quad (16)$$

$$2CH_3CH_2OH_{(v)} \rightarrow (C_2H_5)_2O_{(l)} + H_2O_{(v)} \quad (17)$$

Nickel oxide based materials are efficient catalysts for the ethanol oxidation reaction at high temperatures (500 °C and above), transforming ethanol to methane, CO_x and hydrogen, followed by the water gas shift and methane steam reforming, approaching the equilibrium conditions. Methane is certainly critical, limiting the formation of hydrogen at low and intermediate temperatures. Therefore, steam reforming reaction for production of hydrogen need higher temperatures. However, under such conditions, the water gas shift reaction inhibits the hydrogen production. In fact, NiO promotes the methane formation by decomposition of ethanol (Eq. (16)).

Acetaldehyde derives from the oxidative dehydrogenation of ethanol and in most cases occurs over strong basic sites, such as O^{2-} or HOO^- and at low temperatures. Ethylene is an undesirable byproduct of the partial oxidation of ethanol and besides the dehydration of ethanol occurring on acid sites provokes the dissociation of ethanol functional group with the formation of olefins,

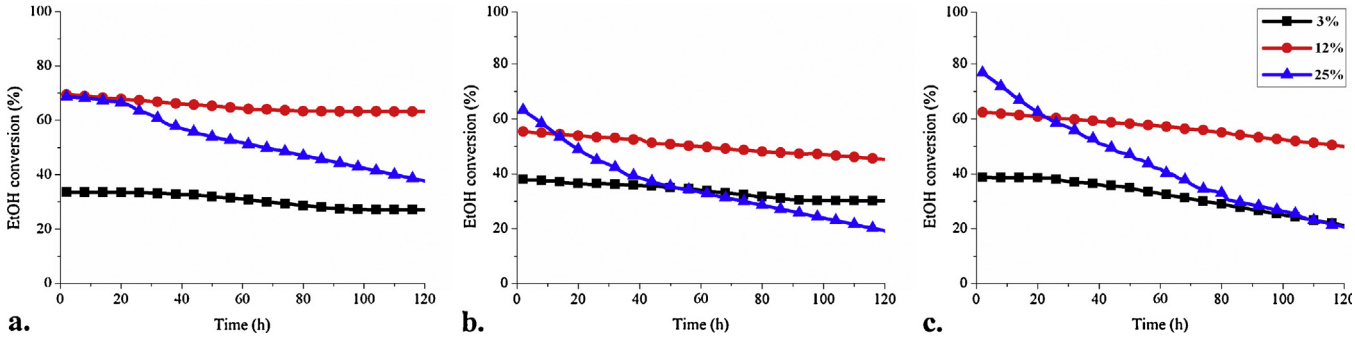

Fig. 7. Test stability of supported metal oxides (a) Co_3O_4 (b) NiO and (c) CuO on stream at 3, 12 and 25 (%, w/w).

causing deactivation of the catalyst. Indeed, high temperatures (520–770 °C) have been used for complete conversion of ethanol [20–23]. Table 5 presents the selectivity of carbon-based products, consisting mainly of CO and CH_4. The H_2 selectivity increased significantly, probably due to ethanol decomposition reaction in the gas phase (Eq. (16)).

4.1.1. Diffuse reflectance infrared spectroscopy analyses(DRIFTS)

DRIFTS analysis of ethanol oxidation reaction was performed for all catalysts with 12% metal oxide supported on γ-Al_2O_3. These catalysts exhibited the best stability and the results are presented in Fig. 9.

The absorption bands located between 3780 cm^{-1} and 3790 cm^{-1} are related to the stretching movement of OH groups, and eventually coordinated to water molecules on the oxide surface, derived from oxidation reaction, especially at low temperatures when significant amounts of water molecules are linked at the surface level. Temperature increment showed increasing H_2 consumption from ambient temperature up to 420 °C, which is related to the reduction of the metal oxides.

Bands at 3020 cm^{-1} and between 1300 cm^{-1} and 1350 cm^{-1} indicate the presence of methane with strong stretching signals of C—H bond, as reported previously [34]. Small bands between 2340 cm^{-1} and 2350 cm^{-1} are associated to the stretching vibration of average strength of the O═C═O bonds, suggesting the presence of carbon dioxide entrapped in the pores of the oxides, showing that its concentration changed along time, which represents the selectivity of the oxidation reaction to CO_2. In fact, the Co_3O_4 oxide presents the most important change in terms of CO_2 concentration, presenting the highest CO and O_2 conversion and CO_2 selectivity, followed by NiO and CuO oxide respectively. Bands between 2170 cm^{-1} and 2180 cm^{-1} are related to the presence of C—O and C═O bonds due to asymmetric stretching movement for CO and CO_2 molecules in the region of 1400–1550 cm^{-1}, which are important signals corresponding to strong stretching of C—O bond.

Bands between 1600 cm^{-1} and 1675 cm^{-1} are related to olefins and confirm the presence of ethylene on all supported oxides. The presence of aldehyde can be distinguished by examining both, the presence of the C—H of aldehyde bands around 2750–2850 cm^{-1} and of a carbonyl groups, however, as displayed in Fig. 9, the eventual presence of this compounds is relatively low and not consistent with the results derived from the catalytic tests, where the selectivity of ethylene and acetaldehyde are about 8.6% and 27.7%, respectively. Finally, the bands between 725 cm^{-1} and 1180 cm^{-1}, corresponding to the C—O bond stresses are associated to acetals (traces of acetaldehyde and ketones) and saturated primary alcohols (ethanol fractions). The bending out of the plane and band changes at lower frequencies (~1100 → 1180–1170) is assigned to ν(C—OH) species [30].

4.1.2. Temperature programmed desorption of ethanol (TPD-Ethanol)

Fig. 10 shows the TPD profiles for Co_3O_4, NiO and CuO supported oxides on γ-Al_2O_3. Results confirm the presence of the principal products. In all cases, results allow to identify the main fragments derived from different chemical reactions, occurring during the oxidation and decomposition of ethanol, as shown in Eqs. (10), (12), (13), (16) and (17). At low temperatures there are some traces of ethylene, acetaldehyde, diethyl ether and acetic acid, which could be derived from ethanol fragments or fragments of carboxyl groups desorbed around these temperatures. Rodrigues et al. [20], suggested for lower temperatures the desorption of ethanol, the dehydrogenation forming acetaldehyde followed by cracking

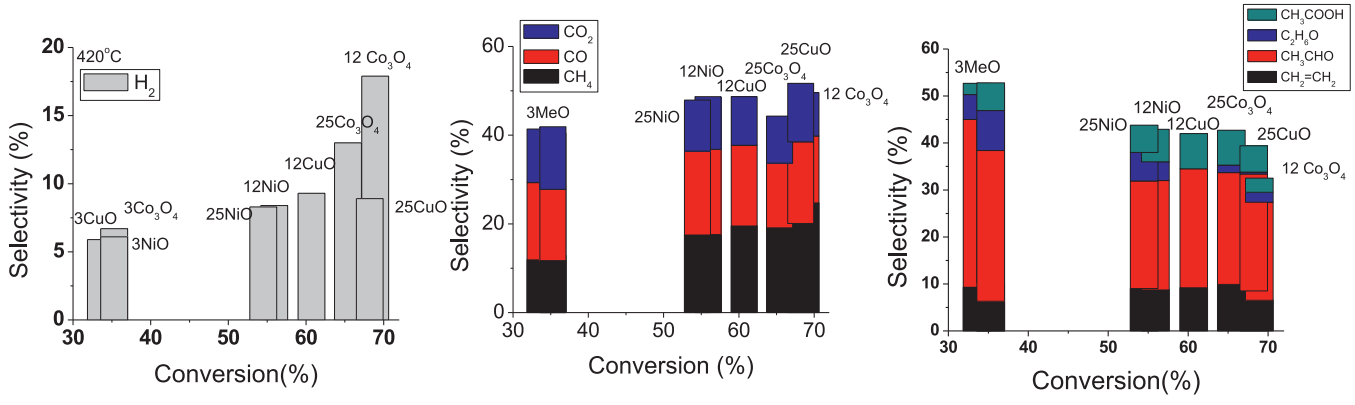

Fig. 8. Diagram bars for (a) Co_3O_4 (b) NiO and (c) CuO supported catalyst at 420 °C with metal oxide concentration.

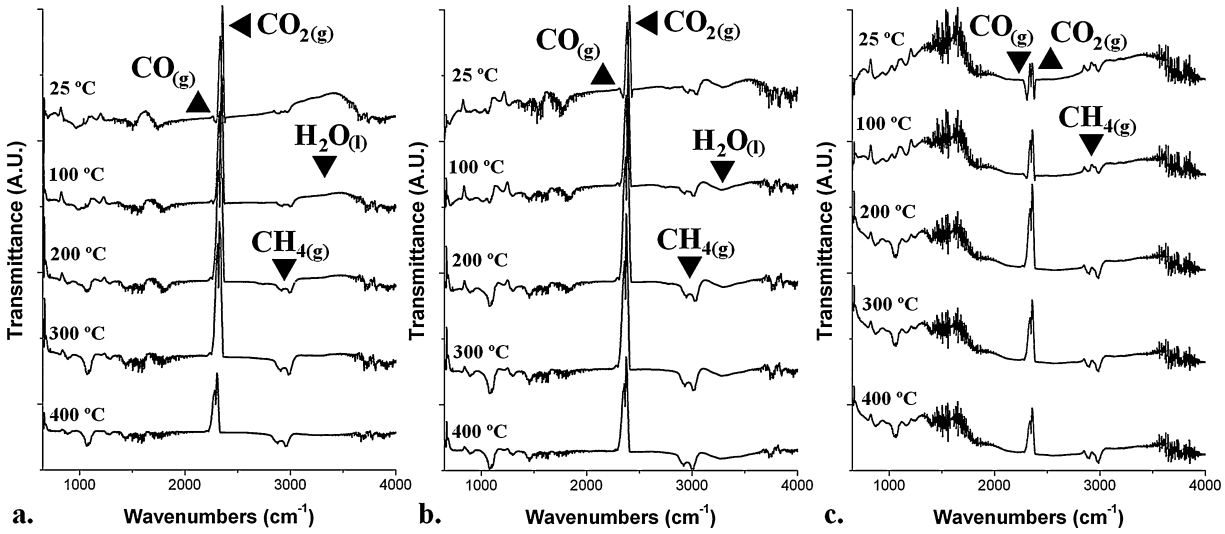

Fig. 9. In situ DRIFTS spectrums of ethanol oxidation reaction for 12% (a) Co_3O_4, (b) NiO and (c) CuO supported metal oxides at different temperatures from room temperature.

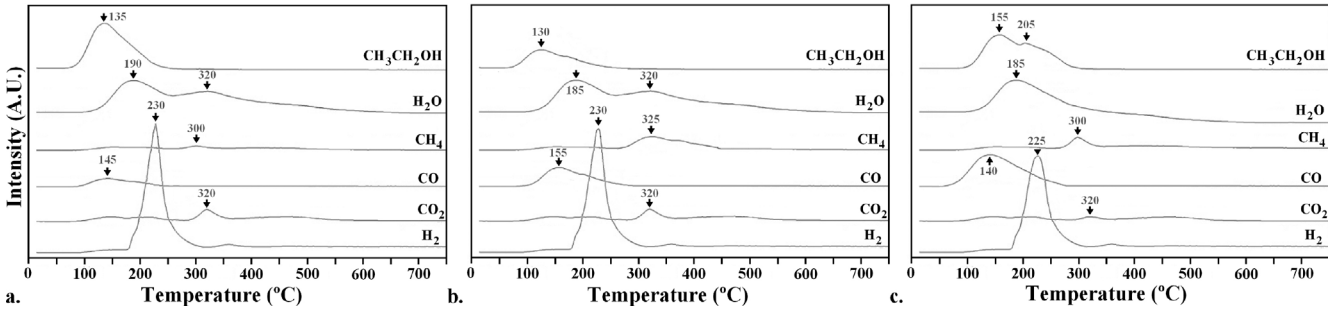

Fig. 10. TPD-ethanol profiles for (a) Co_3O_4, (b) NiO and (c) CuO supported catalyst vs temperature.

producing CO, CH_4, and H_2 as the principal products as shown in Eq. (16).

The dehydrogenation of ethanol occurs at 240 °C with the formation of acetaldehyde, ethylene and diethyl ether fragments with lower intensity, together with desorption of H_2. In fact, the H_2 peak is relatively high at lower temperatures, desorbing at higher temperatures. Beyond 300 °C only few traces of CO, CH_4, and H_2O were observed, in particular over NiO and CuO catalysts.

4.2. Reaction test at 650 °C

The reaction at 650 °C showed high conversions of ethanol, around 90% in comparison with the reaction at low temperature, which is related to the development of coupled reactions, generating H_2, CH_4, CO and CO_2 as principal products. Results derived from gas chromatography, confirm that secondary species as ethylene, acetaldehyde, diethyl ether, acetic acid and acetone between others were reduced until the detection limits, as shown in Table 7. Fig. 11 shows the H_2 selectivity as function of the conversion for 12% MeO at 420 and 650 °C.

For the Co_3O_4 supported catalyst, under the same reactions conditions evaluated at low temperature, it is clear that this oxide induces thermal activation, since ethanol conversion increases proportionally with temperature. The principal products at high temperatures are H_2O, H_2, CH_4, CO and CO_2, as shown in Fig. 12, together with small amounts of acetaldehyde, confirming the decomposition of aldehydes in the gas phase which increases methane. Sahoo et al. [28] observed reduction of CO_2 attributed to the water gas shift reaction, favoring CO formation. Additionally, the selectivity of methane is lower than of hydrogen, suggesting steam reforming of methane.

The conversion of ethanol for NiO is lower than for Co_3O_4, evidencing the formation of secondary products, just observed at low temperatures and attributed to the dehydration of ethanol. The formation of secondary products, such as, ethylene, acetaldehyde, diethyl ether, acetic acid and acetone decreases continuously with increasing temperature [29].

The CuO catalyst presented lower ethanol conversions in comparison with the Co_3O_4 catalyst, which may be related to

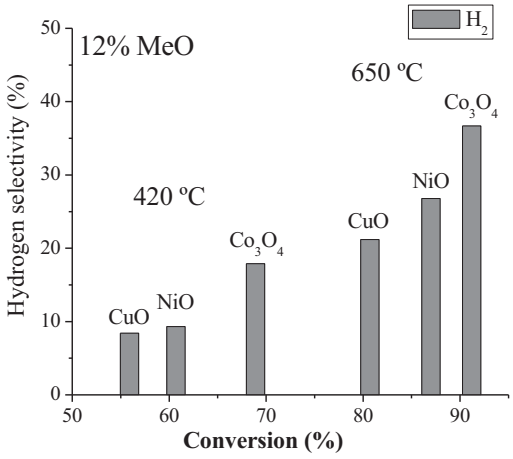

Fig. 11. Hydrogen selectivity as function of the conversion for 12% catalyst at 420 and 650 °C.

Table 7
Ethanol conversion and product distribution on partial oxidation of ethanol over 12% of (a) Co_3O_4, (b) NiO and (c) CuO/γ-Al_2O_3/cordierite catalysts at 650 °C and GSHV = 1.8×10^4 h^{-1}.

12% (w/w)	$X_{ethanol}$ (%)	CO_2/CO	Selectivity (% molar)							
			H_2	CH_4	CO	CO_2	CH_2=CH_2	CH_3CHO	C_2H_6O	CH_3COOH
Co_3O_4	91.2	0.02	36.7	23.3	32.5	0.8	2.7	2.8	0.7	0.5
NiO	87.0	0.04	26.8	24.5	35.9	1.6	3.0	4.9	1.9	1.4
CuO	80.7	0.05	21.2	18.9	40.2	2.6	7.4	7.0	1.2	1.5

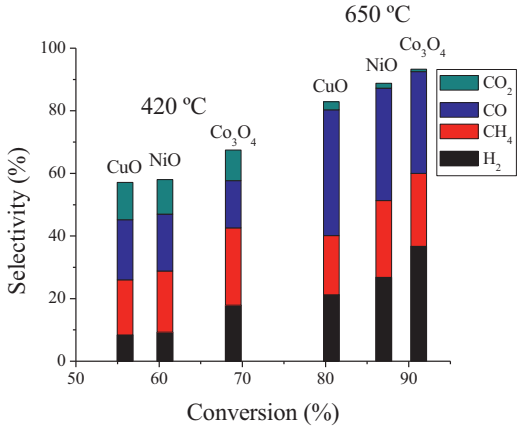

Fig. 12. Selectivity to different products as function of the conversion for 12% catalyst at 420 and 650 °C.

the deactivation phenomena. However, the product distribution, selectivity to synthesis gas is relatively stable. It suggests that acetaldehyde and ethylene are the primary products resulting from the dehydrogenation and dehydration reactions, while the secondary products, like CO and CO_2 from the partial oxidation and water gas shift reactions. It suggests the adsorption of ethanol at the surface in the first step with the formation of $CH_3CH_2O_{(a)}$ groups that are easily transformed in acetaldehyde. In the second step acetaldehyde is oxidized with the formation of acetates that decomposes to CO and CH_4 in gas phase at higher temperatures.

The oxidative dehydrogenation of ethanol forming acetaldehyde is considered an acid reaction that occurs on strong basic sites, such as O^{2-} or HOO^-, and at low reaction temperatures. In this context, among the principal byproducts, ethylene is an unlikely byproduct, inhibiting the acid sites and promoting the dissociation of functional groups during olefin formation [34]. These results are in good agreement with Sheng et al. [26] using a Rh–Pt/CeO_2 catalysts, who observed decreasing in CO_2 production, due to the water gas shift reaction, which reduces the hydrogen production.

5. Conclusions

The preparation method by means of citric acid as complex agent allowed obtaining high dispersion of metal oxide crystallites over washcoated alumina and good adherence over cordierite monoliths. TEM, SEM and XRD analyses confirm the presence of well-structured nanometric crystallites.

The partial oxidation of ethanol was studied at 420 and 650 °C. The conversion of ethanol increased with increasing metal content of Co_3O_4, reaching maximum conversion for 12% MeO and excellent stability.

The reactivity sequence Co_3O_4 > NiO > CuO confirming that cobalt catalyst present most interesting properties for ethanol oxidation. However, the specific activities in terms of metallic surface area for Co_3O_4 and NiO catalysts are of the same order.

The H_2 selectivity increased with temperature and metal content with maximum for 12% MeO/γ-Al_2O_3. The selectivity of acetaldehyde decreased with increasing MeO concentration. Higher MeO concentrations showed fast deactivation due to carbon formation at the surface and unlikely byproducts.

DRIFTS and TPD analyses showed that the formation of different byproducts during the reaction contributed to the progressive deactivation. Acetaldehyde oxidizes forming acetates which than decomposes to form CO and CH_4 in the gas phase at high temperatures.

Acknowledgement

The authors would like to acknowledge to FAPERJ for the financial support provided in project E-26/100.787/2012.

References

[1] P.R. Piscina, N. Homs, J. Chem. Soc. Rev. 37 (2008) 2459–2467.
[2] R.M. Navarro, M.A. Peña, J.L.G. Fierro, Chem. Rev. 107 (2007) 3952–3991.
[3] Z. Al-Hamamre, M.A. Hararah, Int. J. Hydrogen Energy 35 (2010) 5367–5377.
[4] L.V. Mattos, F.B. Noronha, J. Catal. 233 (2005) 453–463.
[5] J.R. Salge, G.A. Deluga, L.D. Schmidt, J. Catal. 235 (2005) 69–78.
[6] S.M. Lima, A.M. Silva, L.O. Costa, U.M. Graham, G. Jacobs, B.H. Davis, L. Mattos, F. Noronha, J. Catal. 268 (2009) 268–281.
[7] W. Wang, Z. Wang, Y. Ding, J. Xi, G. Lu, J. Catal. Lett. 81 (2002) 63–68.
[8] A. Haryanto, S. Fernando, N. Murali, S. Adhikari, Energy Fuels 19 (2005) 2098–2106.
[9] L.V. Mattos, F.B. Noronha, J. Power Sources 152 (2005) 50–59.
[10] A.M. Silva, L.O. Costa, A.P.M.G. Barandas, L.E.P. Borges, L.V. Mattos, F.B. Noronha, J. Catal. Today 133 (2008) 755–761.
[11] K.L. Hohn, L.D. Schmidt, J. Appl. Catal. 211 (2001) 53–68.
[12] A.L. Alberton, M.M.V.M. Souza, M. Schmal, Catal. Today 123 (2007) 257–264.
[13] G.A. Deluga, J.R. Salge, L.D. Schmidt, X.E. Verykios, J. Science 303 (2004) 993–997.
[14] A.N. Fatsikostas, D.I. Kondarides, X.E. Verykios, J. Catal. Today 75 (2002) 145–155.
[15] D.K. Liguras, K. Goundani, X.E. Verykios, J. Power Sources 130 (2004) 30–37.
[16] A. Pestryakov, V.V. Lunin, A.N. Devochkin, J. Appl. Catal. A: Gen. 227 (2002) 125–130.
[17] A.M. Silva, A.P.M. Barandas, J. Catal. Today 129 (2007) 297–304.
[18] E.C. Wanat, B. Suman, L.D. Schmidt, J. Catal. 235 (2005) 18–27.
[19] E.B. Pereira, N. Homs, S. Martí, J. Catal. 257 (2008) 206–214.
[20] C.P. Rodrigues, M. Schmal, Int. J. Hydrogen Energy 36 (2011) 10709–10718.
[21] J.J. Kingsley, L.R. Pederson, J. Mater. Res. Proc. 296 (1992) 296–361.
[22] G. Avgouropoulos, T. Ioannides, J. Appl. Catal. A: Gen. 244 (2003) 155–167.
[23] G. Avgouropoulos, J. Papavasiliou, T. Tabakova, V. Idakiev, T. Ioannides, J. Chem. Eng. 124 (2006) 41–45.
[24] C.P. Rodrigues, V. Teixeira, M. Schmal, J. Appl. B: Catal. Environ. 96 (2010) 1–9.
[25] A. Casanovas, C. Leitenburg, A. Trovarelli, J. Catal. Today 138 (2008) 187–192.
[26] P.Y. Sheng, A. Yee, J. Catal. 208 (2002) 393–403.
[27] W. Wang, Z. Wang, J. Catal. Lett. 81 (2002) 63–68.
[28] D.R. Sahoo, S. Vajpai, J. Chem. Eng. 125 (2007) 139–147.
[29] M. Schmal, D.V. Cesar, M.V. Souza, C.E. Guarido, Can. J. Chem. Eng. 89 (5) (2011) 1166–1175.
[30] J.A. Gómez-Cuaspud, M. Schmal, Int. J. Hydrogen Energy 38 (2013) 7458–7468.
[31] A.Y. Khodakov, J. Appl. Catal. A: Gen. 254 (2003) 273–288.
[32] (a) D.I. Enache, B. Rebours, M. Roy-Auberger, R.J. Revel, J. Catal. 205 (2002) 345–346;
(b) C. Perdomo-Rodrigues, M. Schmal, Int. J. Hydrogen Energy 36 (2011) 10709–10718.
[33] J. Llorca, N. Homs, J. Sales, P.F. Piscina, J. Catal. 209 (2002) 306–317.
[34] R.W. McCabe, P.J. Mitchell, J. Eng. Chem. Prod. Res. 23 (1984) 196–202.